Supplementary

Design of Multicomponent Argyrodite Based on a Mixed Oxidation State as Promising Solid-State Electrolyte using Moment Tensor Potentials

Ji Won Lee[a], Ji Hoon Kim[a], Ji Seon Kim[a], Yong Jun Jang[b], Sun Ho Choi[b], Seong Hyeon Choi[b], Sung Man Cho[b], Yong-Gu Kim[b], and Sang Uck Lee[a,*]

[a]*School of Chemical Engineering, Sungkyunkwan University, Suwon 16419, Republic of Korea*

[b]*Hyundai Motor Company, Hwasung-si, Gyeonggi-do 18280, Republic of Korea*

*Corresponding authors Email: suleechem@skku.edu (Sang Uck Lee)

Keywords: Solid-state electrolyte; Argyrodite; Mixed Oxidation State; Multicomponent; Ionic conductivity; Chemical Stability; Moment tensor potential

Supplementary Note S1

Structural information

Pristine halogenated Li-argyrodite (Li_6PS_5D [D = Cl, Br, I]) has cubic unit cells and can be specifically expressed as $[Li_6^+][PS_4]^{3-}[S^{2-}D^-]$ as shown in Figure S1(a). PS_4^{3-} polyhedrons are located at 4b sites, and Li fully occupies 24g sites and partially occupies 48h sites, which are cage-like forms. Single S^{2-} and D^- anions are located at 4a or 4c sites in the half-void form, (shaped as if inside a Li-cage). For theoretical research, atoms of the crystal structures should be fully occupied. So, we used "enumlib" code (http://github.com/msg-byu/enumlib)[1-4] to define Li-ion occupancy by generating derivate symmetrical and distinct superstructures of a parent lattice. In the case of multicomponent argyrodite ($Li_{5+2x+y}[A]_x^{4+}[B]_y^{5+}[C]_{1-x-y}^{6+}S_5[D]$) systems, we considered variation in the total number of Li ions (Li_{5+2x+y}) depends on the type of mixed cation with different oxidation states ($[A]_x^{4+}[B]_y^{5+}[C]_{1-x-y}^{6+}$).

Moreover, we consider the 4a and 4c sites of eight single anions (four S^{2-} and four X^-), that are divided into ordered and disordered structures, because the halogenated Li-argyrodite (Li_6PS_5D [D = Cl, Br, I]) can have six as ordered and disordered configurations depending on 4a-4c site disorder of S^{2-} and X^- single anions, as shown in Figure S1(b). The ordered $0\%(F\bar{4}3m)$, $100\%(F\bar{4}3m)$ structures indicate the percentage of site occupancy of X^- at the 4c site, which is full of single anions of one kind. On the other side, the disordered $25\%(R3m)$, $50\%(P2_122, P2mm)$, $75\%(R3m)$ structures also indicate the percentage of site occupancy D^- at the 4c site. The 50% disorder case is divided into 2 cases with the same percentage of site occupancy D^- at the 4c but different positions. However, in our previous research, we found that I^- prefers a fully ordered configuration with 100% occupancy at 4a site compared to disordered occupancy of both 4a and 4c sites for Cl^- or Br^-. So, we used only fully ordered configuration for iodine-based Li-argyrodite and all six configurations for Cl^- or Br^--based Li-argyrodite.

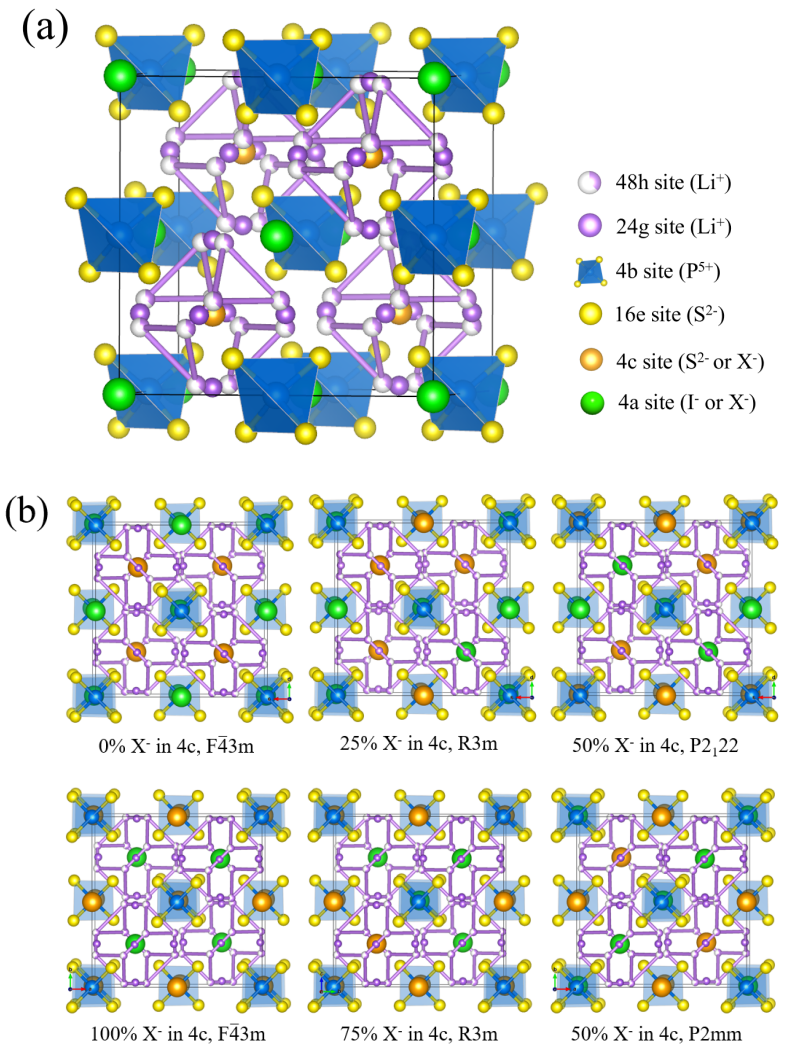

Figure S1. (a) Crystal structure and Wyckoff position of halogenated Li-argyrodite (Li_6PS_5D [D = Cl, Br, I]). (b) Six configurations of argyrodite according to site occupancy D^- at the 4c site. Each percentage indicates the D^- occupancy at the 4c site. The green circle indicates the position of D^- at the 4c site.

Supplementary Note S2

Workflow of MTP development

The processes involved in machine-learned moment tensor potential (MTP) development[5] are illustrated in Figure S1 with seven steps including training set generation of all possible potential energy surfaces in the configuration space, MTP training based on DFT energies, and MD simulations for ionic conductivities. Snapshot extractions were performed with pymatgen[6] and MTP training was performed by MLIP[7, 8] and a materials machine learning (MAML)[9] python package.

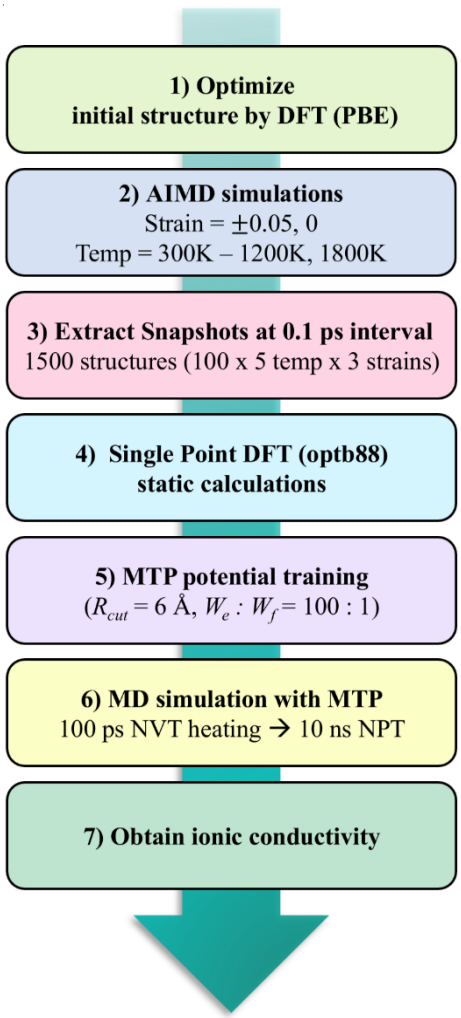

Figure S2. Machine-learned moment tensor potential (MTP) development workflow for evaluating ionic conductivity (σ_{RT}).

S2-1. Generation of training sets

We preferentially performed geometric optimization of our bulk structures using the Perdew–Burke–Ernzerohf (PBE) functional, and then generated strained structures in all lattice directions with ±5% strain to ensure diversity. However, the generated strained structures cannot sufficiently cover a potential energy surface in the configurational space for accurate MTP development. To consider most structural diversity in configurational space, we generated an amorphous structure with *ab initio* molecular dynamics (AIMD) simulations using an NVT Nose-Hoover thermostat[10, 11] at four temperatures of 300K, 600K, 900K, 1200K, and 1800K during 10 ps with a 2 fs timestep. In these short AIMD simulations, a total of 1,500 snapshots were extracted and used as a training set to cover most configurational space. We then made single-point density functional theory (DFT) calculations to obtain the energy and force for 1,500 snapshot structures at optB88-vdw level of theory.[12] The calculated results for crystal structure, energy, and force are applied to the following MTP training.

S2-2. MTP training

In the MTP training, we used hyperparameters R_{cut} of 6 Å, $\mathrm{Lev}_{\mathrm{max}}$ of 12, the weights of energy and force of 100:1, and a 9:1 of training sets to validation sets.[13, 14] Based on the hyperparameters, the MTP was fitted to the energy and force of training sets calculated by DFT at optB88-vdw (MTP_optB88-vdw). After MTP training, we confirmed that the mean absolute errors (MAEs) of energy and force were less than 5 meV/atom and 0.09 eV/Å, respectively, as illustrated in Figure S2. The MTP developed in a given composition can be equally applied to any configurations of the same composition.

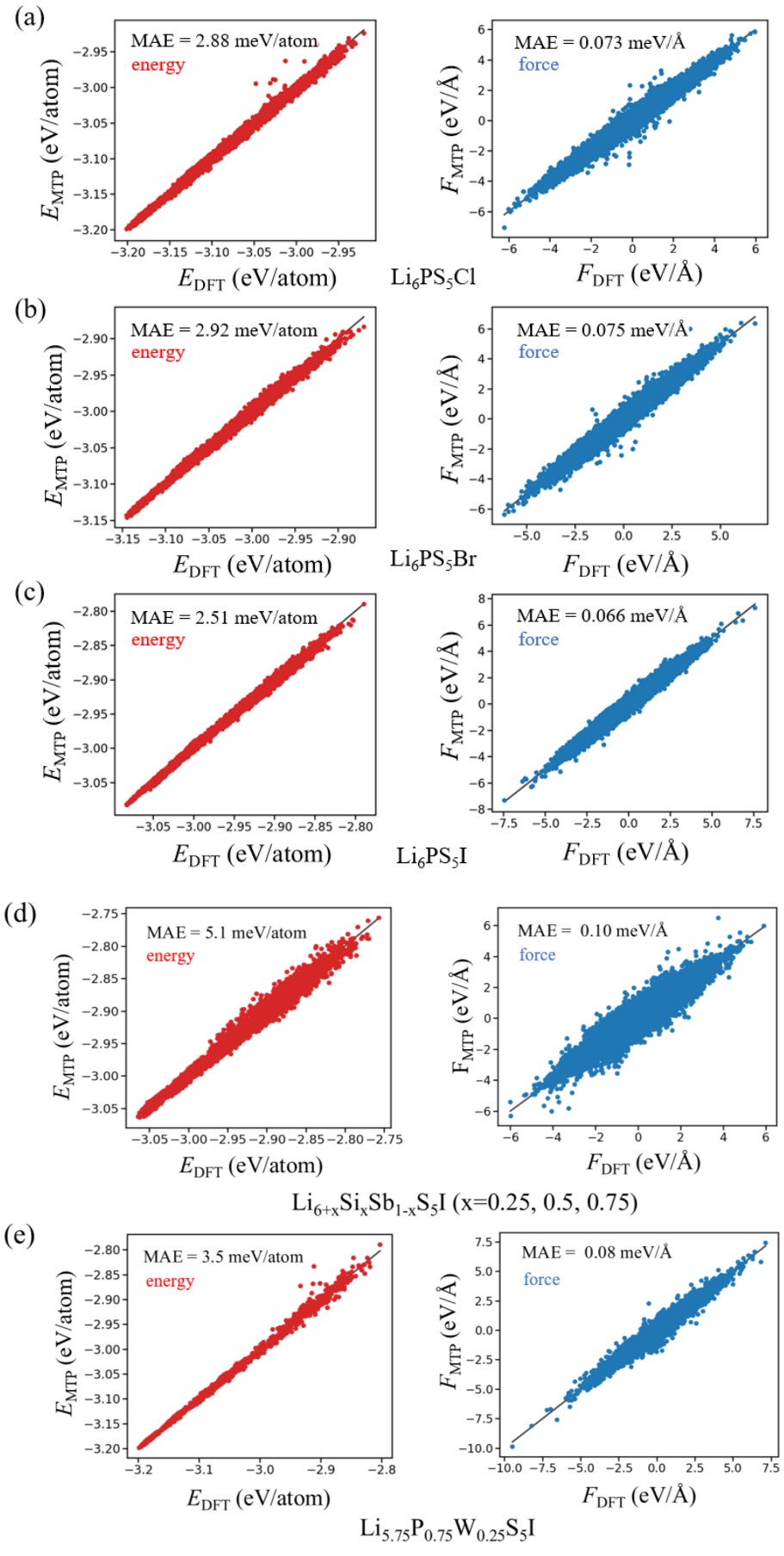
(a)
MAE = 2.88 meV/atom
energy
E_{MTP} (eV/atom)
E_{DFT} (eV/atom)
MAE = 0.073 meV/Å
force
F_{MTP} (eV/Å)
F_{DFT} (eV/Å)
Li_6PS_5Cl
(b)
MAE = 2.92 meV/atom
energy
MAE = 0.075 meV/Å
force
Li_6PS_5Br
(c)
MAE = 2.51 meV/atom
energy
MAE = 0.066 meV/Å
force
Li_6PS_5I
(d)
MAE = 5.1 meV/atom
energy
MAE = 0.10 meV/Å
force
$Li_{6+x}Si_xSb_{1-x}S_5I$ (x=0.25, 0.5, 0.75)
(e)
MAE = 3.5 meV/atom
energy
MAE = 0.08 meV/Å
force
$Li_{5.75}P_{0.75}W_{0.25}S_5I$

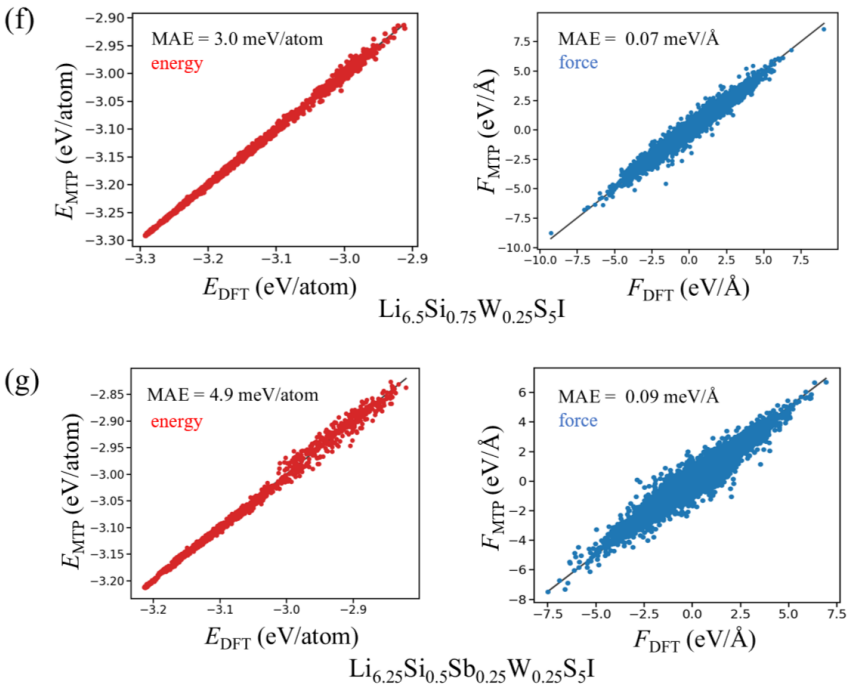

Figure S3. Correlation between MTP- and DFT-based energy and force evaluations for the representative Li-argyrodite systems of (a) Li_6PS_5Cl (b) Li_6PS_5Br (c) Li_6PS_5I (d) $Li_{6+x}Si_xSb_{1-x}S_5I$ (x=0.25, 0.5, 0.75) (e) $Li_{5.75}P_{0.75}W_{0.25}S_5I$ (f) $Li_{6.5}Si_{0.75}W_{0.25}S_5I$, and (g) $Li_{6.25}Si_{0.5}Sb_{0.25}W_{0.25}S_5I$. Each mean absolute error (MAE) is provided in the inset at the upper left of the plot.

S2-3. MD simulation and evaluation of ionic conductivity using MTP

We performed large-scale and long-time MD simulations of 3 × 3 × 3 supercell structures (> 30 Å) at seven temperatures from 350K to 500K at 25K intervals using developed MTP_optB88-vdw and repeated this process twice to generate an ensemble average. The target temperature was obtained by increasing the temperature by 10 K to the target temperature during 100 ps of NVT simulation. After that, the NPT simulation was carried out at a target temperature over 10 ns. Then, the diffusivity was obtained from the mean square displacement (MSD) of twice-repeated NPT simulations, and the ionic conductivities at 300 K (σ_{RT}) was calculated using the Nernst-Einstein relation and Arrhenius fitted diffusivity at each temperature, as shown in Figure S3.

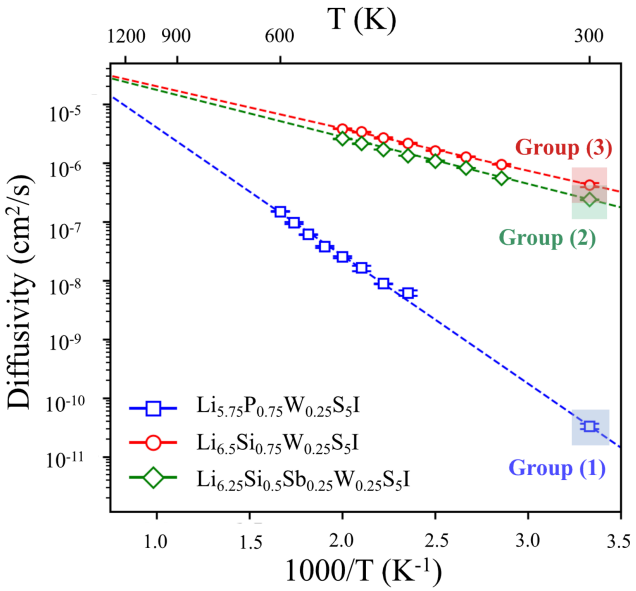

Figure S4. Arrhenius plots of diffusivities calculated by MTP_optB88-vdw of the representative candidates, $Li_{5.75}P_{0.75}W_{0.25}S_5I$, $Li_{6.5}Si_{0.75}W_{0.25}S_5I$, and $Li_{6.25}Si_{0.5}Sb_{0.25}W_{0.25}S_5I$, at temperatures range from 350 K to 500 K for extrapolated diffusivity at 300 K.

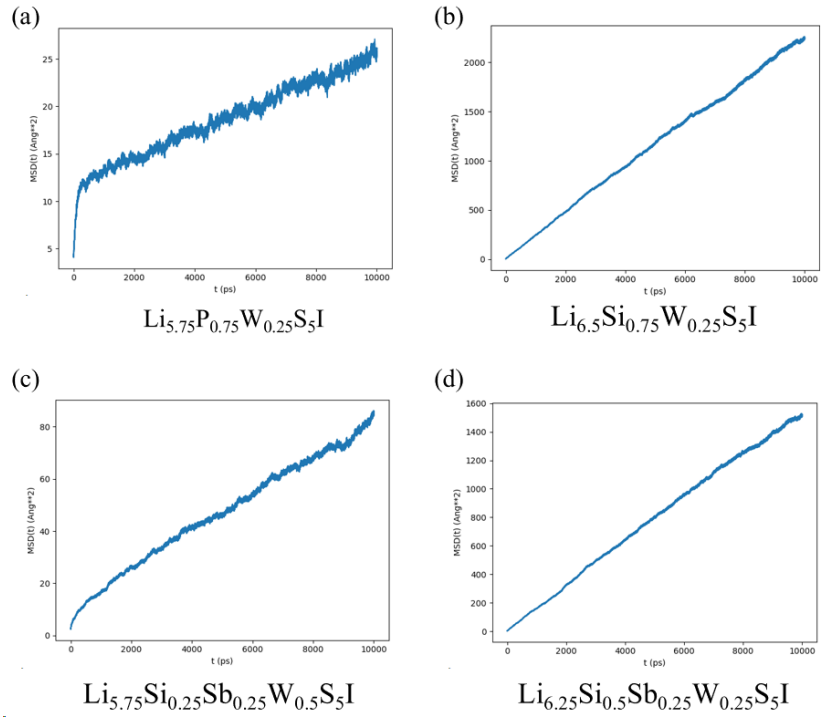

Figure S5. MSD plots of Li ion calculated by MTP_optB88-vdw of the representative candidates, $Li_{5.75}P_{0.75}W_{0.25}S_5I$, $Li_{6.5}Si_{0.75}W_{0.25}S_5I$, $Li_{5.75}Si_{0.25}Sb_{0.25}W_{0.5}S_5I$, and $Li_{6.25}Si_{0.5}Sb_{0.25}W_{0.25}S_5I$ at 500K.

S2-4. MTP validation

To verify the accuracy of the developed MTP_optB88-vdw, we compared the calculated σ_{RT} with the already reported experimentally observed values of Li_6PS_5D[15-18,19] (D= Cl, Br, I), $Li_{6+x}Si_xSb_{1-x}S_5I$ (x=0.25, 0.5 and 0.75)[20], Li_3YCl_6[21] and $Li_7P_3S_{11}$[21]. MTP_optB88-vdw give more accurate σ_{RT} in close agreement with experimental values rather than AIMD results. Therefore, we can assert that the MTP_optB88-vdw based MD simulation is highly acceptable for $\boldsymbol{\sigma_{RT}}$ prediction of Li-argyrodite systems rather than AIMD simulation. In fact, it has been known that AIMD simulations often lead to large discrepancies between predicted and experimentally measured σ_{RT} values due to the high temperatures and short time scales of simulations for small size of systems.[21]

Table S1. Ionic conductivities calculated from AIMD and MTP_optB88-vdw at 300 K (σ_{RT}) compared to experimental values.

Composition	σ_{RT} (mS/cm)		
	AIMD	MTP	Experiments
Li_6PS_5I	0.84[15]	0.001	0.001[17]
Li_6PS_5Cl	4.6[19]	2.46	2.3-2.5[16]
Li_6PS_5Br	3.12[15]	1.59	1.0[18]
$Li_{6.25}Si_{0.25}Sb_{0.75}S_5I$	2.6	10.4	-
$Li_{6.5}Si_{0.5}Sb_{0.5}S_5I$	9.0[20]	13.6	11.6[20]
$Li_{6.75}Si_{0.75}Sb_{0.25}S_5I$	37.9[20]	14.8	13.1[20]
Li_3YCl_6	14[21]	0.56	0.51[21]
$Li_7P_3S_{11}$	57[21]	6.5	4-17[21]

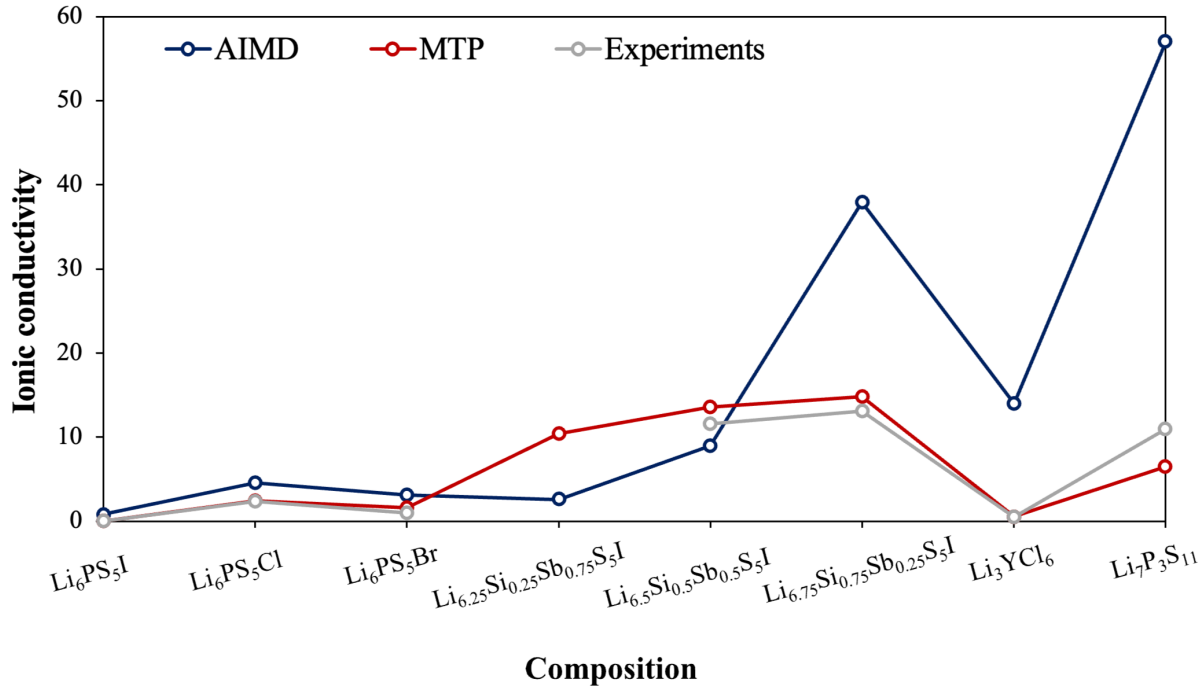

Figure S6. Ionic conductivities calculated from AIMD and MTP_optB88-vdw at 300 K (σ_{RT}) compared to experimental values.

Supplementary Note S3

Evaluating ionic conductivity

To determine the diffusivity (D) of certain ions in the system, we fit the mean square displacements (MSD), which represents the average squared displacements over time against $2dt$, and calculate the motion of mobile ions per unit time using trajectories generated from MD simulations. D and MSD are defined as:

$$D = \frac{1}{2dt}\text{MSD} \qquad \text{Eqn. S1}$$

, where t is the time duration and r_i(t) is the position of a mobile ion. Based on the diffusivity for the target system, the ionic conductivities at room temperature (300K) were evaluated by extrapolating from high-temperature values using Arrhenius fitting due to the diffusivity corresponding to the Arrhenius relationship when no phase transition within the given temperature range. To calculate the ion conductivity at a certain temperature, we used the Arrhenius equation:

$$D = D_0 \exp\left(-\frac{E_a}{kT}\right) \qquad \text{Eqn. S2}$$

, where D_0 is the diffusivity at infinite temperature and E_a is the activation energy of diffusion, which can be obtained through a linear fit of $log(D)$ against $1/T$. The term k is the Boltzmann constant and T is temperature. Ionic conductivity (σ) can then be calculated from the Nernst-Einstein relation:

$$\sigma_T = \frac{\rho z^2 F^2}{RT} D_\mathrm{T} \qquad \text{Eqn. S3}$$

, where ρ is the molar density of mobile ions in the unit cell, and F, R, and z are Faraday's constant, the gas constant, and the charge of mobile ions, respectively. In this study, to satisfy reasonable ergodicity, we repeated MD simulations twice for the same structure and temperature. Consequently, the estimated ionic conductivity at room temperature (σ_{RT}) is calculated as the average of ionic conductivities extrapolated to room temperature in all MD simulations.

Table S2. Chemical formula and indices of all simulated structures, and ionic conductivities at 300 K (σ_{RT}) calculated from MTP_optB88-vdw

Group	Structure Index	Chemical formula	Ionic conductivity (mS/cm)
	*	Li_6PS_5I	0.001
Group (1)	1	$Li_{5.75}P_{0.75}Mo_{0.25}S_5I$	0.004
	2	$Li_{5.25}P_{0.25}Mo_{0.75}S_5I$	0.004
	3	$Li_{5.5}P_{0.5}Mo_{0.5}S_5I$	0.005
	4	$Li_{5.75}P_{0.75}W_{0.25}S_5I$	0.01
	5	$Li_{5.25}Sb_{0.25}Mo_{0.75}S_5I$	0.016
	6	$Li_{5.25}P_{0.25}W_{0.75}S_5I$	0.02
	7	$Li_{5.5}P_{0.5}W_{0.5}S_5I$	0.06
	8	$Li_{5.5}Sb_{0.5}W_{0.5}S_5I$	0.11
	9	$Li_{5.25}Sb_{0.25}W_{0.75}S_5I$	0.14
	10	$Li_{5.75}Sb_{0.75}W_{0.25}S_5I$	0.19
	11	$Li_{5.75}Sb_{0.75}Mo_{0.25}S_5I$	0.23
	12	$Li_{5.5}Sb_{0.5}Mo_{0.5}S_5I$	0.46
Group (2)	13	$Li_{5.5}Si_{0.25}W_{0.75}S_5I$	0.21
	14	$Li_{5.5}Ge_{0.25}Mo_{0.75}S_5I$	0.25
	15	$Li_6Si_{0.5}W_{0.5}S_5I$	0.3
	16	$Li_{5.5}Ge_{0.25}W_{0.75}S_5I$	0.33
	17	$Li_6Sn_{0.5}Mo_{0.5}S_5I$	0.97
	18	$Li_6Si_{0.5}Mo_{0.5}S_5I$	1.03
	19	$Li_{5.5}Si_{0.25}Mo_{0.75}S_5I$	1.25
	20	$Li_{5.5}Sn_{0.25}W_{0.75}S_5I$	1.88
	21	$Li_6Ge_{0.5}W_{0.5}S_5I$	2.22
	22	$Li_{5.5}Sn_{0.25}Mo_{0.75}S_5I$	2.98
	23	$Li_6Sn_{0.5}W_{0.5}S_5I$	3.94
	24	$Li_{6.5}Sn_{0.75}W_{0.25}S_5I$	4.2
	25	$Li_6Ge_{0.5}Mo_{0.5}S_5I$	5.5
	26	$Li_{6.5}Sn_{0.75}Mo_{0.25}S_5I$	5.74
	27	$Li_{6.5}Ge_{0.75}Mo_{0.25}S_5I$	27.14
	28	$Li_{6.5}Ge_{0.75}W_{0.25}S_5I$	51.98
	29	$Li_{6.5}Si_{0.75}Mo_{0.25}S_5I$	52.14
	30	$Li_{6.5}Si_{0.75}W_{0.25}S_5I$	62.93
Group (3)	31	$Li_6Si_{0.25}Sb_{0.5}Mo_{0.25}S_5I$	0.06
	32	$Li_6Ge_{0.25}Sb_{0.5}W_{0.25}S_5I$	0.06
	33	$Li_6Sn_{0.25}Sb_{0.5}W_{0.25}S_5I$	0.07
	34	$Li_6Sn_{0.25}Sb_{0.5}Mo_{0.25}S_5I$	0.11
	35	$Li_6Si_{0.25}Sb_{0.5}W_{0.25}S_5I$	0.16
	36	$Li_6Ge_{0.25}Sb_{0.5}Mo_{0.25}S_5I$	0.21
	37	$Li_{5.75}Si_{0.25}Sb_{0.25}Mo_{0.5}S_5I$	0.3

	38	$Li_{5.75}Si_{0.25}Sb_{0.25}W_{0.5}S_5I$	0.4
	39	$Li_{5.75}Sn_{0.25}Sb_{0.25}Mo_{0.5}S_5I$	0.81
	40	$Li_{5.75}Ge_{0.25}Sb_{0.25}Mo_{0.5}S_5I$	0.86
	41	$Li_{5.75}Sn_{0.25}Sb_{0.25}W_{0.5}S_5I$	0.95
	42	$Li_{5.75}Ge_{0.25}Sb_{0.25}W_{0.5}S_5I$	1.27
	43	$Li_{6.25}Sn_{0.5}Sb_{0.25}Mo_{0.25}S_5Is$	6.22
	44	$Li_{6.25}Sn_{0.5}Sb_{0.25}W_{0.25}S_5I$	7.56
	45	$Li_{6.25}Ge_{0.5}Sb_{0.25}W_{0.25}S_5I$	14.93
	46	$Li_{6.25}Ge_{0.5}Sb_{0.25}Mo_{0.25}S_5I$	16.35
	47	$Li_{6.25}Si_{0.5}Sb_{0.25}Mo_{0.25}S_5I$	33.05
	48	$Li_{6.25}Si_{0.5}Sb_{0.25}W_{0.25}S_5I$	33.74
Group (4-1)	49	$Li_{6.25}Ge_{0.5}Sb_{0.25}W_{0.25}S_5Br$	13.84
	50	$Li_{6.5}Ge_{0.75}Mo_{0.25}S_5Br$	16.41
	51	$Li_{6.25}Si_{0.5}Sb_{0.25}Mo_{0.25}S_5Br$	16.87
	52	$Li_{6.5}Ge_{0.75}W_{0.25}S_5Cl$	18.4
	53	$Li_{6.5}Si_{0.75}W_{0.25}S_5Br$	19.82
	54	$Li_{6.25}Ge_{0.5}Sb_{0.25}Mo_{0.25}S_5Cl$	20.28
	55	$Li_{6.25}Ge_{0.5}Sb_{0.25}Mo_{0.25}S_5Br$	20.57
	56	$Li_{6.25}Si_{0.5}Sb_{0.25}W_{0.25}S_5Br$	21.64
	57	$Li_{6.25}Ge_{0.5}Sb_{0.25}W_{0.25}S_5Cl$	21.75
	58	$Li_{6.5}Si_{0.75}W_{0.25}S_5Cl$	22.79
	59	$Li_{6.5}Ge_{0.75}W_{0.25}S_5Br$	24.87
	60	$Li_6Si_{0.75}W_{0.25}S_{4.5}Cl_{1.0}Br_{0.5}$	26.09
	61	$Li_{6.5}Si_{0.75}Mo_{0.25}S_5Cl$	26.24
	62	$Li_6Ge_{0.75}W_{0.25}S_{4.5}Cl_{1.0}Br_{0.5}$	30.5
	63	$Li_{6.25}Si_{0.5}Sb_{0.25}W_{0.25}S_5Cl$	30.6
	64	$Li_{6.5}Ge_{0.75}Mo_{0.25}S_5Cl$	31.24
	65	$Li_{6.25}Si_{0.5}Sb_{0.25}Mo_{0.25}S_5Cl$	31.65
	66	$Li_{6.5}Si_{0.75}Mo_{0.25}S_5Br$	38.03
Group (4-2)	67	$Li_{5.75}Ge_{0.5}Sb_{0.25}Mo_{0.25}S_{4.5}Cl_{1.0}Br_{0.5}$	38.28
	68	$Li_{5.75}Ge_{0.5}Sb_{0.25}Mo_{0.25}S_{4.5}Cl_{0.5}Br_{1.0}$	51.06
	69	$Li_6Ge_{0.75}Mo_{0.25}S_{4.5}Cl_{0.5}Br_{1.0}$	51.61
	70	$Li_{5.75}Ge_{0.5}Sb_{0.25}W_{0.25}S_{4.5}Cl_{0.5}Br_{1.0}$	53.27
	71	$Li_{5.75}Si_{0.5}Sb_{0.25}W_{0.25}S_{4.5}Br_{1.0}Cl_{0.5}$	55.47
	72	$Li_{5.75}Si_{0.5}Sb_{0.25}Mo_{0.25}S_{4.5}Br_{1.0}Cl_{0.5}$	63.74
	73	$Li_{5.75}Si_{0.5}Sb_{0.25}Mo_{0.25}S_{4.5}Cl_{1.0}Br_{0.5}$	65.23
	74	$Li_6Si_{0.75}W_{0.25}S_{4.5}Cl_{0.5}Br_{1.0}$	67.66
	75	$Li_{5.75}Si_{0.5}Sb_{0.25}W_{0.25}S_{4.5}Cl_{1.0}Br_{0.5}$	72.52
	76	$Li_6Ge_{0.75}W_{0.25}S_{4.5}Cl_{0.5}Br_{1.0}$	72.85
	77	$Li_{5.75}Ge_{0.5}Sb_{0.25}W_{0.25}S_{4.5}Cl_{1.0}Br_{0.5}$	75.68
	78	$Li_6Si_{0.75}Mo_{0.25}S_{4.5}Cl_{1.0}Br_{0.5}$	76.25
	79	$Li_6Si_{0.75}Mo_{0.25}S_{4.5}Cl_{0.5}Br_{1.0}$	80.32

	80	$Li_{5.75}Ge_{0.75}Mo_{0.25}S_{4.25}Cl_{1.25}Br_{0.5}$	0.03
	81	$Li_{5.5}Ge_{0.5}Sb_{0.25}W_{0.25}S_{4.25}Cl_{1.25}Br_{0.5}$	0.47
Group (4-3)	82	$Li_{5.5}Si_{0.5}Sb_{0.25}Mo_{0.25}S_{4.25}Cl_{1.25}Br_{0.5}$	0.89
	83	$Li_{5.5}Si_{0.5}Sb_{0.25}W_{0.25}S_{4.25}Cl_{1.25}Br_{0.5}$	2.38
	84	$Li_{5.5}Ge_{0.5}Sb_{0.25}Mo_{0.25}S_{4.25}Cl_{1.25}Br_{0.5}$	7.72

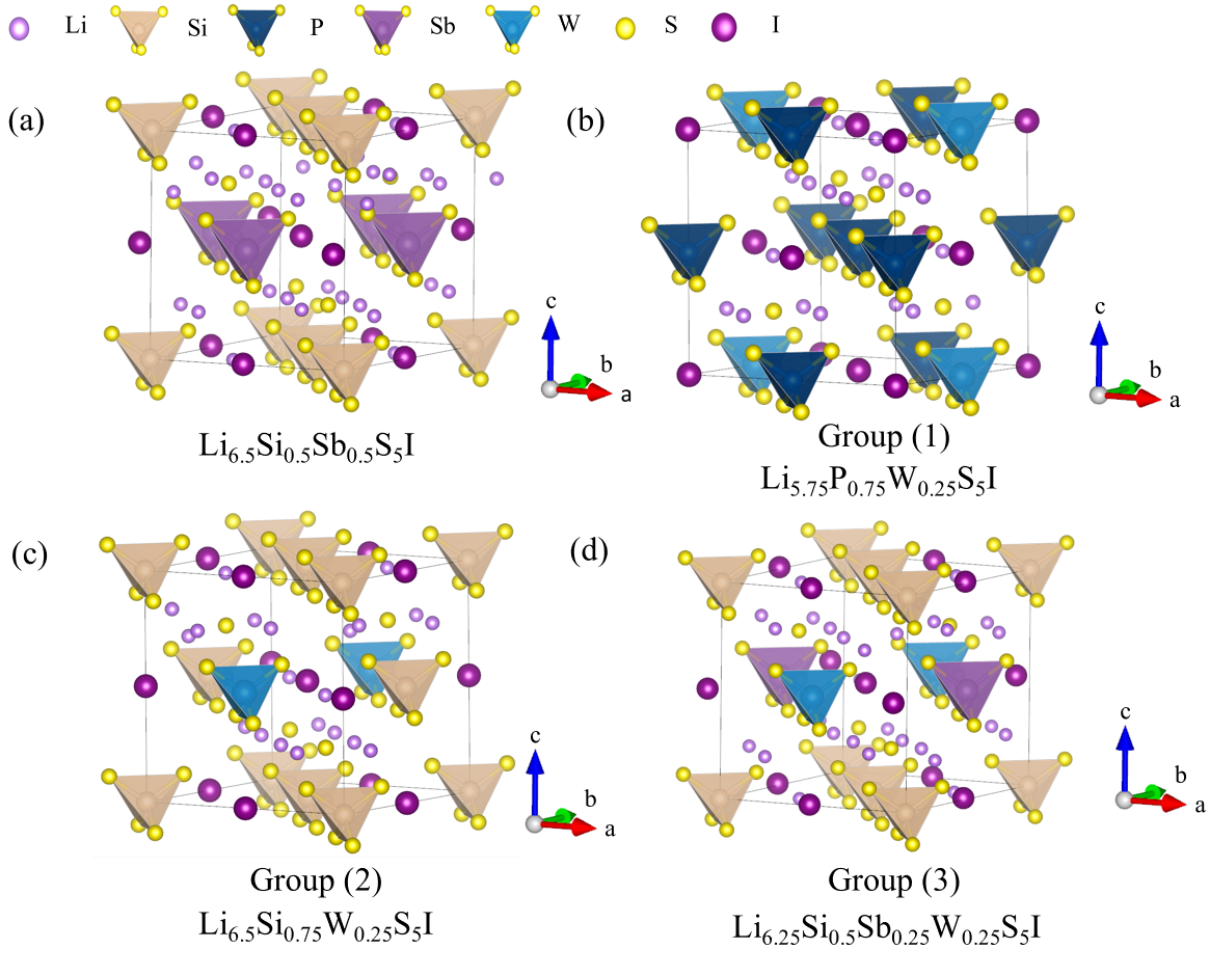

Figure S7. Crystal structures of representative Li-argyrodite (a) $Li_{6.5}Si_{0.5}Sb_{0.5}S_5I$, (b) $Li_{5.75}P_{0.75}W_{0.25}S_5I$, (c) $Li_{6.5}Si_{0.75}W_{0.25}S_5I$, and (d) $Li_{6.25}Si_{0.5}Sb_{0.25}W_{0.25}S_5I$.

Supplementary Note S4

van Hove correlation function

The van Hove distribution function can be employed to analyze information about the correlation in ion diffusion.[22] The van Hove distribution function is defined as the probability of ions moving *r* from their original position during a given time *t* and it can usually be separated into a self-part (G_s) and a distinct-part (G_d) as follows:

$$G(r,t) = \frac{1}{N}\left\langle \sum_{i=1}^{N} \delta\big(r + r_i(0) - r_i(t)\big) \right\rangle + \frac{1}{N}\left\langle \sum_{i \neq j}^{N} \delta\left(r + r_j(0) - r_i(t)\right) \right\rangle$$

$$\equiv G_s(r,t) + G_d(r,t) \qquad \text{Eqn. S4}$$

Here, $\langle \cdot \rangle$ is an ensemble average and $\delta(\cdot)$ is the three-dimensional Dirac delta function. G_s represents the distance the ion has traveled from its initial position after time *t* has passed. Therefore, if a strong peak appears at the same distance for a long time, the ion diffusion does not happen properly. G_d provides information on the movement of the remaining *N*-1 ions, revealing the speed at which the reference ion site is replaced by other ions. In this study, the van Hove correlation function was obtained using pymatgen-diffusion code implemented on pymatgen.[6, 23]

Supplementary Note S5

Random structure calculation

The configuration within the bulk structure of argyrodite differs according to the degree of thermodynamic stability of the structure. The structure with the highest thermodynamic stability occupies the largest portion of the configuration within the bulk structure. To account for this influence, we constructed 3 × 3 × 3 supercell structures of argyrodite, in which each configuration is randomly distributed based on thermodynamic stability. The allocation of numbers based on thermodynamic stability was determined using the following equation:

$$Number\ of\ site = P_i(E) * n_s\ /\ sum\ of\ P_i(E) \qquad \text{Eqn. S5}$$

, where n_s is the total number of sites. We designed a 3 × 3 × 3 supercell that contains 27 unit cells, and so we set the value of n_s to 27. If the sum of all sites is less than or greater than n_s, the most stable structure is removed or 1 site is added. The generation of structures was obtained using pymatgen.[6] Because the relatively large size of I^- prefers a fully ordered configuration with 100% occupancy at 4a site compared to the disordered occupancy of both 4a and 4c sites for Cl^- and Br^-, we used all six configurations for Cl and Br-based models and only 1 ordered configuration for I-based model.

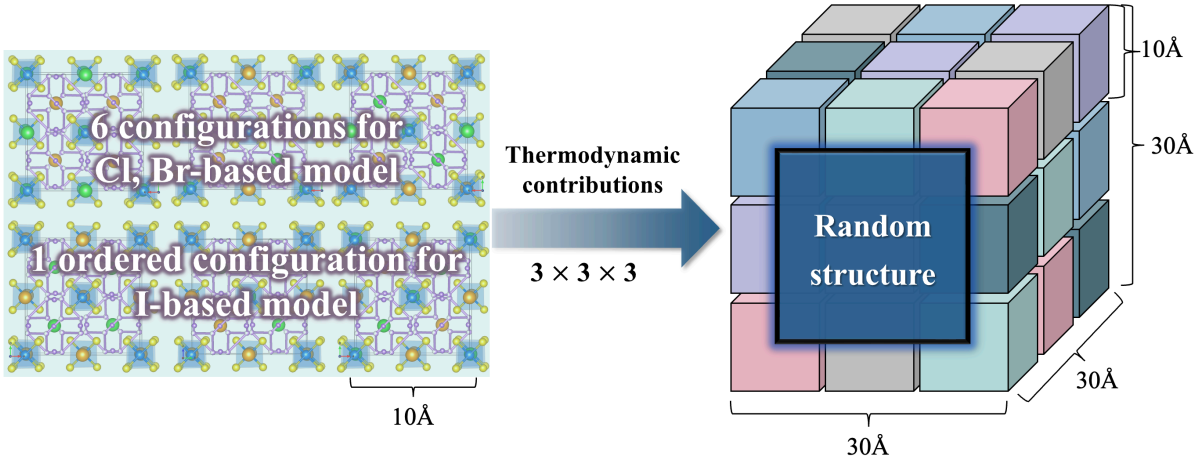

Figure S8. Schematic of a 3 × 3 × 3 supercell structure composed of 27 unit-cells considering the thermodynamic stability of the six characteristic configurations.

Supplementary Note S6

Chemical stability of electrode interfacial reaction and hydrolysis

Many experimental studies have provided evidence for the interfacial decomposition and the formation of interphase layers at the solid-state electrolytes (SSE)-electrode interfaces. The chemical reactions between the SSE and the electrode materials caused by the chemical incompatibility between the SSE and the electrodes. And the interfacial degradation results in high interfacial resistance at the SSE-electrode interface, which is an important problem in all-solid-state batteries (ASSBs) and limits the power and rate performance of ASSBs. In addition, a major challenge in large-scale fabrication of sulfide-based SSEs is their poor stability against moisture in the air. Even trace amounts of moisture in the surrounding environment can initiate spontaneous hydrolysis reactions for many lithium thiophosphates, deteriorating the material and its properties and releasing toxic H_2S gas. Therefore, excellent electrode interfacial stability and air stability are required for the development of sulfide SSEs.

To address the issues of electrode interfacial stability and air stability, we calculated the interface reaction and H_2S formation energies based on the compositional phase diagrams using the pymatgen package.[6] In evaluating the chemical stability of interfaces, we considered the interface as a pseudo-binary[24, 25] of the SSE and the electrode, which has a composition of

$$C_{\text{interface}}(C_{SSE}, C_{electrode}, x) = x \cdot C_{SSE} + (1 - x)C_{electrode} \qquad \text{Eqn. S6}$$

where C_{SSE} and $C_{electrode}$ are the compositions of SSE and electrode materials, respectively, and x is the molar fraction of the SSE varying from 0 to 1. The energy of the interface pseudo-binary

$$C_{\text{interface}}(SSE,\text{electrode}, x) = x \cdot E(SSE) + (1 - x)E(electrode) \qquad \text{Eqn. S7}$$

was set to a linear combination of the electrolyte and electrode energies. The decomposition energy (ΔE_D) of the interface pseudo-binary was calculated as

$$\Delta E_D(SSE,\text{electrode},x) = E_{eq}\left(C_{interface}(C_{SSE},C_{electrode},x)\right) - E_{interface}(SSE,electrode,x) \quad \text{Eqn. S8}$$

The air stability evaluation also follows same process based on pseudo-binary reaction equation defined as

$$C_{\text{products}}(SSE,\text{H}_2\text{O},x) = x\cdot C(\text{SSE}) + (1-x)C(\text{H}_2\text{O}) \quad \text{Eqn. S9}$$

The hydrolysis reaction energy can be calculated as

$$E_{\text{reaction}}(SSE,\text{H}_2\text{O},x) = E_{\text{eq}}\left(C_{\text{products}}(SSE,\text{H}_2\text{O},x)\right) - E\left(C_{\text{products}}(SSE,\text{H}_2\text{O},x)\right) \quad \text{Eqn. S10}$$

, where $E_{eq}(C)$ means the energy minimum of the phase equilibria at given composition.

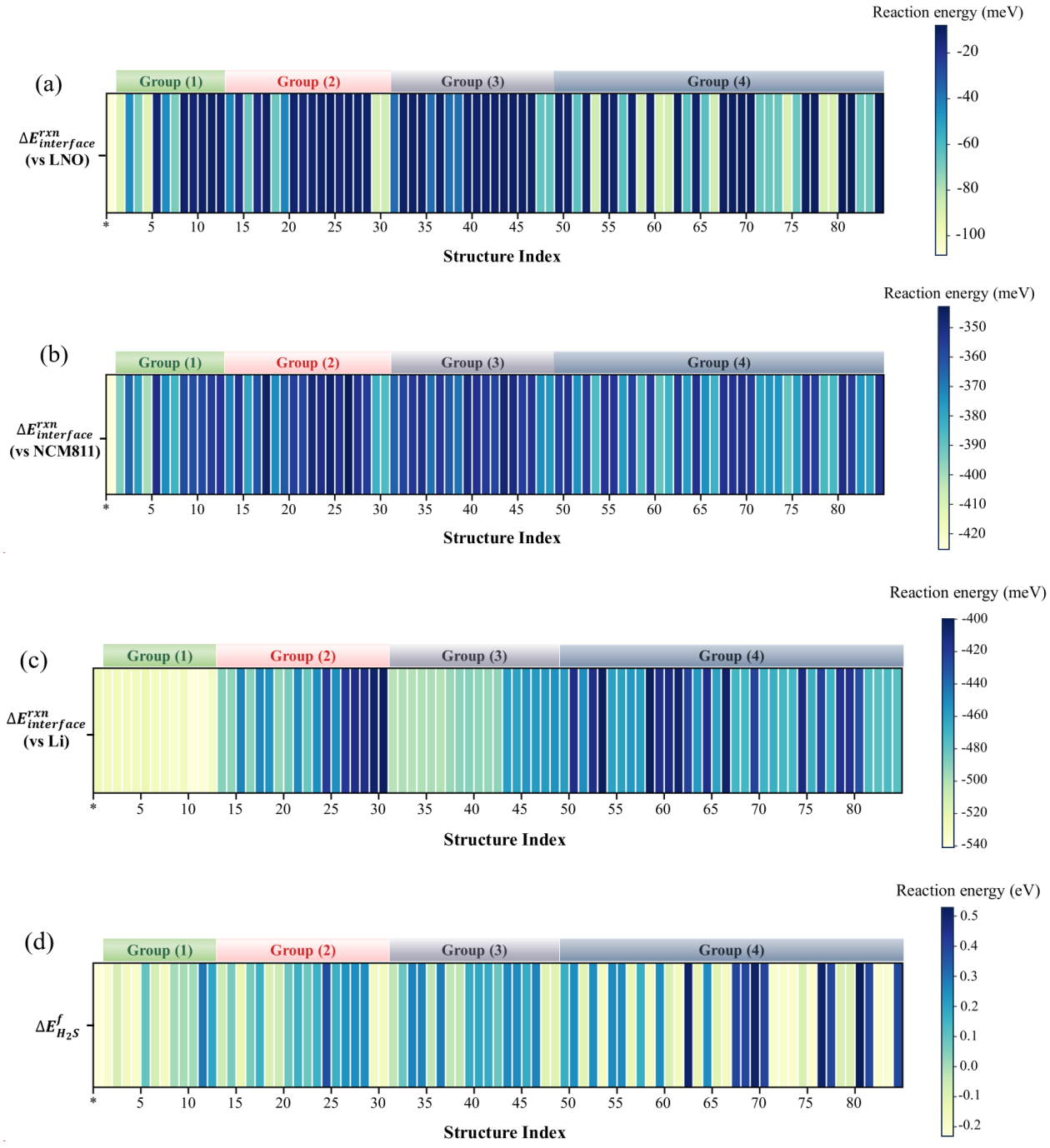

Figure S9. Heatmap plot of calculated interface reaction energy ($\Delta E^{rxn}_{interface}$) for all structures at the interface with (a) LNO ($LiNbO_3$) coating material, (b) $LiNi_{0.8}Co_{0.1}Mn_{0.1}O_2$ (NCM 811) cathode and (c) Li anode, and (d) H_2S formation energy ($\Delta E^{f}_{H_2S}$), according to Groups.

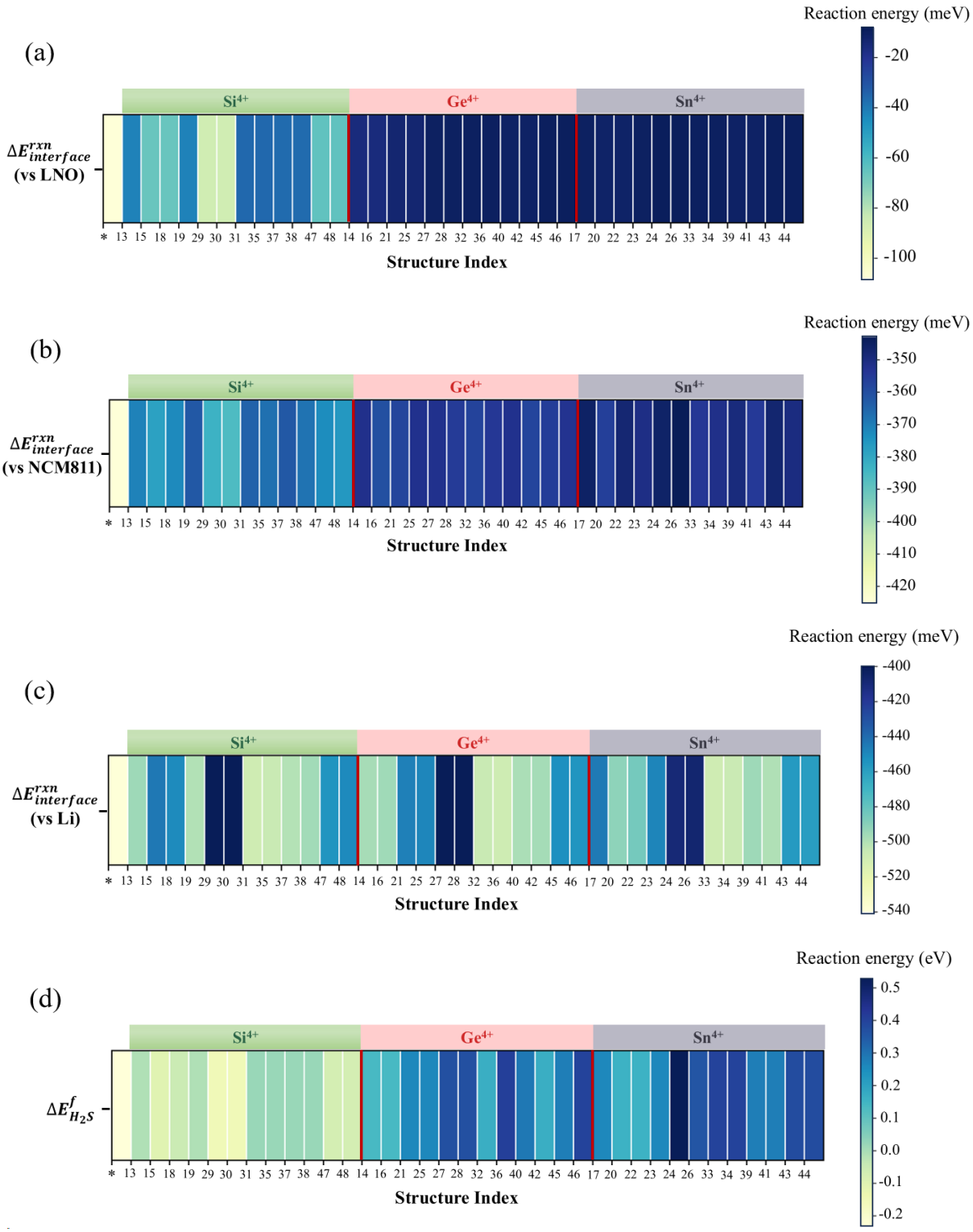

Figure S10. Heatmap plot illustrating the significantly improved chemical stability of Sn^{4+} and Ge^{4+} in $[A]^{4+}$

Table S3. The calculated interface reaction energy ($\Delta E_{interface}^{rxn}$) of all structures at the interface with LNO ($LiNbO_3$) coating material, $LiNi_{0.8}Co_{0.1}Mn_{0.1}O_2$ (NCM 811) cathode, and (c) Li anode.

Group	Structure Index	Structure	$\Delta E_{interface}^{rxn}$ (meV)		
			LNO	NCM811	Li
	*	Li_6PS_5I	-107.55	-424.46	-539.24
Group (1)	1	$Li_{5.75}P_{0.75}Mo_{0.25}S_5I$	-90.74	-394.36	-540.69
	2	$Li_{5.25}P_{0.25}Mo_{0.75}S_5I$	-44.29	-364.36	-541.19
	3	$Li_{5.5}P_{0.5}Mo_{0.5}S_5I$	-69.73	-377.10	-542.38
	4	$Li_{5.75}P_{0.75}W_{0.25}S_5I$	-90.74	-400.00	-540.63
	5	$Li_{5.25}Sb_{0.25}Mo_{0.75}S_5I$	-11.99	-351.20	-535.96
	6	$Li_{5.25}P_{0.25}W_{0.75}S_5I$	-44.29	-373.00	-543.74
	7	$Li_{5.5}P_{0.5}W_{0.5}S_5I$	-69.73	-383.40	-542.13
	8	$Li_{5.5}Sb_{0.5}W_{0.5}S_5I$	-10.93	-358.91	-548.82
	9	$Li_{5.25}Sb_{0.25}W_{0.75}S_5I$	-11.99	-359.55	-541.67
	10	$Li_{5.75}Sb_{0.75}W_{0.25}S_5I$	-9.69	-358.27	-555.43
	11	$Li_{5.75}Sb_{0.75}Mo_{0.25}S_5I$	-9.69	-355.51	-553.67
	12	$Li_{5.5}Sb_{0.5}Mo_{0.5}S_5I$	-10.93	-353.36	-545.15
Group (2)	13	$Li_{5.5}Si_{0.25}W_{0.75}S_5I$	-41.98	-370.55	-499.5
	14	$Li_{5.5}Ge_{0.25}Mo_{0.75}S_5I$	-15.67	-351.92	-501.58
	15	$Li_6Si_{0.5}W_{0.5}S_5I$	-65.82	-377.92	-453.51
	16	$Li_{5.5}Ge_{0.25}W_{0.75}S_5I$	-15.67	-360.24	-500.06
	17	$Li_6Sn_{0.5}Mo_{0.5}S_5I$	-10.18	-345.26	-453.92
	18	$Li_6Si_{0.5}Mo_{0.5}S_5I$	-65.82	-372.24	-459.7
	19	$Li_{5.5}Si_{0.25}Mo_{0.75}S_5I$	-41.98	-361.94	-503.82
	20	$Li_{5.5}Sn_{0.25}W_{0.75}S_5I$	-11.31	-355.84	-495.82
	21	$Li_6Ge_{0.5}W_{0.5}S_5I$	-13.14	-357.59	-455.86
	22	$Li_{5.5}Sn_{0.25}Mo_{0.75}S_5I$	-11.31	-347.50	-490.05
	23	$Li_6Sn_{0.5}W_{0.5}S_5I$	-10.18	-350.84	-457.63
	24	$Li_{6.5}Sn_{0.75}W_{0.25}S_5I$	-8.88	-345.80	-421.93
	25	$Li_6Ge_{0.5}Mo_{0.5}S_5I$	-13.14	-352.08	-457.83
	26	$Li_{6.5}Sn_{0.75}Mo_{0.25}S_5I$	-8.88	-343.00	-420.13
	27	$Li_{6.5}Ge_{0.75}Mo_{0.25}S_5I$	-10.32	-352.23	-414.39
	28	$Li_{6.5}Ge_{0.75}W_{0.25}S_5I$	-10.32	-354.97	-414.46
	29	$Li_{6.5}Si_{0.75}Mo_{0.25}S_5I$	-86.06	-382.82	-404.65
	30	$Li_{6.5}Si_{0.75}W_{0.25}S_5I$	-86.06	-386.19	-400.29
Group (3)	31	$Li_6Si_{0.25}Sb_{0.5}Mo_{0.25}S_5I$	-35.56	-364.22	-511.89
	32	$Li_6Ge_{0.25}Sb_{0.5}W_{0.25}S_5I$	-9.58	-356.94	-509.43
	33	$Li_6Sn_{0.25}Sb_{0.5}W_{0.25}S_5I$	-9.58	-354.14	-511.67
	34	$Li_6Sn_{0.25}Sb_{0.5}Mo_{0.25}S_5I$	-9.58	-351.38	-509.87

	35	$Li_6Si_{0.25}Sb_{0.5}W_{0.25}S_5I$	-35.56	-367.07	-509.03
	36	$Li_6Ge_{0.25}Sb_{0.5}Mo_{0.25}S_5I$	-9.58	-354.18	-511.02
	37	$Li_{5.75}Si_{0.25}Sb_{0.25}Mo_{0.5}S_5I$	-36.2	-362.03	-504.43
	38	$Li_{5.75}Si_{0.25}Sb_{0.25}W_{0.5}S_5I$	-36.2	-367.75	-500.3
	39	$Li_{5.75}Sn_{0.25}Sb_{0.25}Mo_{0.5}S_5I$	-10.82	-349.22	-499.4
	40	$Li_{5.75}Ge_{0.25}Sb_{0.25}Mo_{0.5}S_5I$	-10.82	-352.04	-502.33
	41	$Li_{5.75}Sn_{0.25}Sb_{0.25}W_{0.5}S_5I$	-10.82	-354.76	-503.16
	42	$Li_{5.75}Ge_{0.25}Sb_{0.25}W_{0.5}S_5I$	-10.82	-357.57	-500.82
	43	$Li_{6.25}Sn_{0.5}Sb_{0.25}Mo_{0.25}S_5I$	-9.47	-347.15	-464.85
	44	$Li_{6.25}Sn_{0.5}Sb_{0.25}W_{0.25}S_5I$	-9.47	-349.93	-466.64
	45	$Li_{6.25}Ge_{0.5}Sb_{0.25}W_{0.25}S_5I$	-9.47	-355.61	-461.04
	46	$Li_{6.25}Ge_{0.5}Sb_{0.25}Mo_{0.25}S_5I$	-9.47	-352.87	-463.1
	47	$Li_{6.25}Si_{0.5}Sb_{0.25}Mo_{0.25}S_5I$	-64.35	-372.99	-463.11
	48	$Li_{6.25}Si_{0.5}Sb_{0.25}W_{0.25}S_5I$	-64.35	-375.82	-458.92
Group (4-1)	49	$Li_{6.25}Ge_{0.5}Sb_{0.25}W_{0.25}S_5Br$	-10.43	-356.29	-463.74
	50	$Li_{6.5}Ge_{0.75}Mo_{0.25}S_5Br$	-10.32	-352.23	-414.39
	51	$Li_{6.25}Si_{0.5}Sb_{0.25}Mo_{0.25}S_5Br$	-63.36	-373.68	-456.89
	52	$Li_{6.5}Ge_{0.75}W_{0.25}S_5Cl$	-10.32	-354.97	-414.46
	53	$Li_{6.5}Si_{0.75}W_{0.25}S_5Br$	-86.06	-386.19	-400.29
	54	$Li_{6.25}Ge_{0.5}Sb_{0.25}Mo_{0.25}S_5Cl$	-10.43	-353.54	-465.88
	55	$Li_{6.25}Ge_{0.5}Sb_{0.25}Mo_{0.25}S_5Br$	-10.43	-353.54	-465.88
	56	$Li_{6.25}Si_{0.5}Sb_{0.25}W_{0.25}S_5Br$	-63.36	-376.51	-461.7
	57	$Li_{6.25}Ge_{0.5}Sb_{0.25}W_{0.25}S_5Cl$	-10.43	-356.29	-463.74
	58	$Li_{6.5}Si_{0.75}W_{0.25}S_5Cl$	-86.06	-386.19	-400.29
	59	$Li_{6.5}Ge_{0.75}W_{0.25}S_5Br$	-10.32	-354.97	-414.46
	60	$Li_6Si_{0.75}W_{0.25}S_{4.5}Cl_{1.0}Br_{0.5}$	-88.62	-389.51	-411.73
	61	$Li_{6.5}Si_{0.75}Mo_{0.25}S_5Cl$	-86.06	-382.82	-404.65
	62	$Li_6Ge_{0.75}W_{0.25}S_{4.5}Cl_{1.0}Br_{0.5}$	-8.5	-354.05	-425.26
	63	$Li_{6.25}Si_{0.5}Sb_{0.25}W_{0.25}S_5Cl$	-63.36	-376.51	-461.7
	64	$Li_{6.5}Ge_{0.75}Mo_{0.25}S_5Cl$	-10.32	-352.23	-414.39
	65	$Li_{6.25}Si_{0.5}Sb_{0.25}Mo_{0.25}S_5Cl$	-63.36	-373.68	-465.89
	66	$Li_{6.5}Si_{0.75}Mo_{0.25}S_5Br$	-86.06	-382.82	-404.65
Group (4-2)	67	$Li_{5.75}Ge_{0.5}Sb_{0.25}Mo_{0.25}S_{4.5}Cl_{1.0}Br_{0.5}$	-8.62	-352.49	-478.64
	68	$Li_{5.75}Ge_{0.5}Sb_{0.25}Mo_{0.25}S_{4.5}Cl_{0.5}Br_{1.0}$	-8.62	-352.49	-478.64
	69	$Li_6Ge_{0.75}Mo_{0.25}S_{4.5}Cl_{0.5}Br_{1.0}$	-8.5	-351.05	-425.67
	70	$Li_{5.75}Ge_{0.5}Sb_{0.25}W_{0.25}S_{4.5}Cl_{0.5}Br_{1.0}$	-8.62	-355.50	-476.11
	71	$Li_{5.75}Si_{0.5}Sb_{0.25}W_{0.25}S_{4.5}Br_{1.0}Cl_{0.5}$	-65.43	-377.82	-474.35
	72	$Li_{5.75}Si_{0.5}Sb_{0.25}Mo_{0.25}S_{4.5}Br_{1.0}Cl_{0.5}$	-65.43	-374.69	-478.65
	73	$Li_{5.75}Si_{0.5}Sb_{0.25}Mo_{0.25}S_{4.5}Cl_{1.0}Br_{0.5}$	-65.43	-374.69	-478.65
	74	$Li_6Si_{0.75}W_{0.25}S_{4.5}Cl_{0.5}Br_{1.0}$	-88.62	-389.51	-411.73
	75	$Li_{5.75}Si_{0.5}Sb_{0.25}W_{0.25}S_{4.5}Cl_{1.0}Br_{0.5}$	-65.43	-377.82	-474.35
	76	$Li_6Ge_{0.75}W_{0.25}S_{4.5}Cl_{0.5}Br_{1.0}$	-8.5	-354.05	-425.26

	77	$Li_{5.75}Ge_{0.5}Sb_{0.25}W_{0.25}S_{4.5}Cl_{1.0}Br_{0.5}$	-8.62	-355.50	-476.11
	78	$Li_6Si_{0.75}Mo_{0.25}S_{4.5}Cl_{1.0}Br_{0.5}$	-88.62	-385.04	-416.21
	79	$Li_6Si_{0.75}Mo_{0.25}S_{4.5}Cl_{0.5}Br_{1.0}$	-88.62	-385.04	-416.21
Group (4-3)	80	$Li_{5.75}Ge_{0.75}Mo_{0.25}S_{4.25}Cl_{1.25}Br_{0.5}$	-7.26	-350.37	-431.64
	81	$Li_{5.5}Ge_{0.5}Sb_{0.25}W_{0.25}S_{4.25}Cl_{1.25}Br_{0.5}$	-7.37	-355.03	-482.54
	82	$Li_{5.5}Si_{0.5}Sb_{0.25}Mo_{0.25}S_{4.25}Cl_{1.25}Br_{0.5}$	-66.52	-375.28	-485.3
	83	$Li_{5.5}Si_{0.5}Sb_{0.25}W_{0.25}S_{4.25}Cl_{1.25}Br_{0.5}$	-66.52	-378.59	-480.93
	84	$Li_{5.5}Ge_{0.5}Sb_{0.25}Mo_{0.25}S_{4.25}Cl_{1.25}Br_{0.5}$	-7.37	-351.84	-485.29

Table S4. The calculated H_2S formation energy ($\Delta E^f_{H_2S}$) of all structures.

Group	Structure Index	Structure	$\Delta E^f_{H_2S}$ (eV)
	*	Li_6PS_5I	-0.23
Group (1)	1	$Li_{5.75}P_{0.75}Mo_{0.25}S_5I$	-0.18
	2	$Li_{5.25}P_{0.25}Mo_{0.75}S_5I$	-0.03
	3	$Li_{5.5}P_{0.5}Mo_{0.5}S_5I$	-0.15
	4	$Li_{5.75}P_{0.75}W_{0.25}S_5I$	-0.18
	5	$Li_{5.25}Sb_{0.25}Mo_{0.75}S_5I$	0.18
	6	$Li_{5.25}P_{0.25}W_{0.75}S_5I$	-0.03
	7	$Li_{5.5}P_{0.5}W_{0.5}S_5I$	-0.15
	8	$Li_{5.5}Sb_{0.5}W_{0.5}S_5I$	0.07
	9	$Li_{5.25}Sb_{0.25}W_{0.75}S_5I$	0.06
	10	$Li_{5.75}Sb_{0.75}W_{0.25}S_5I$	0.07
	11	$Li_{5.75}Sb_{0.75}Mo_{0.25}S_5I$	0.42
	12	$Li_{5.5}Sb_{0.5}Mo_{0.5}S_5I$	0.30
Group (2)	13	$Li_{5.5}Si_{0.25}W_{0.75}S_5I$	-0.01
	14	$Li_{5.5}Ge_{0.25}Mo_{0.75}S_5I$	0.14
	15	$Li_6Si_{0.5}W_{0.5}S_5I$	-0.10
	16	$Li_{5.5}Ge_{0.25}W_{0.75}S_5I$	0.14
	17	$Li_6Sn_{0.5}Mo_{0.5}S_5I$	0.26
	18	$Li_6Si_{0.5}Mo_{0.5}S_5I$	-0.05
	19	$Li_{5.5}Si_{0.25}Mo_{0.75}S_5I$	-0.01
	20	$Li_{5.5}Sn_{0.25}W_{0.75}S_5I$	0.16
	21	$Li_6Ge_{0.5}W_{0.5}S_5I$	0.26
	22	$Li_{5.5}Sn_{0.25}Mo_{0.75}S_5I$	0.16
	23	$Li_6Sn_{0.5}W_{0.5}S_5I$	0.26
	24	$Li_{6.5}Sn_{0.75}W_{0.25}S_5I$	0.53
	25	$Li_6Ge_{0.5}Mo_{0.5}S_5I$	0.26
	26	$Li_{6.5}Sn_{0.75}Mo_{0.25}S_5I$	0.36
	27	$Li_{6.5}Ge_{0.75}Mo_{0.25}S_5I$	0.37
	28	$Li_{6.5}Ge_{0.75}W_{0.25}S_5I$	0.37
	29	$Li_{6.5}Si_{0.75}Mo_{0.25}S_5I$	-0.15
	30	$Li_{6.5}Si_{0.75}W_{0.25}S_5I$	-0.15
Group (3)	31	$Li_6Si_{0.25}Sb_{0.5}Mo_{0.25}S_5I$	0.02
	32	$Li_6Ge_{0.25}Sb_{0.5}W_{0.25}S_5I$	0.17
	33	$Li_6Sn_{0.25}Sb_{0.5}W_{0.25}S_5I$	0.40
	34	$Li_6Sn_{0.25}Sb_{0.5}Mo_{0.25}S_5I$	0.40
	35	$Li_6Si_{0.25}Sb_{0.5}W_{0.25}S_5I$	0.02
	36	$Li_6Ge_{0.25}Sb_{0.5}Mo_{0.25}S_5I$	0.41
	37	$Li_{5.75}Si_{0.25}Sb_{0.25}Mo_{0.5}S_5I$	0.02
	38	$Li_{5.75}Si_{0.25}Sb_{0.25}W_{0.5}S_5I$	0.02

	39	$Li_{5.75}Sn_{0.25}Sb_{0.25}Mo_{0.5}S_5I$	0.28
	40	$Li_{5.75}Ge_{0.25}Sb_{0.25}Mo_{0.5}S_5I$	0.29
	41	$Li_{5.75}Sn_{0.25}Sb_{0.25}W_{0.5}S_5I$	0.28
	42	$Li_{5.75}Ge_{0.25}Sb_{0.25}W_{0.5}S_5I$	0.17
	43	$Li_{6.25}Sn_{0.5}Sb_{0.25}Mo_{0.25}S_5I$	0.38
	44	$Li_{6.25}Sn_{0.5}Sb_{0.25}W_{0.25}S_5I$	0.38
	45	$Li_{6.25}Ge_{0.5}Sb_{0.25}W_{0.25}S_5I$	0.28
	46	$Li_{6.25}Ge_{0.5}Sb_{0.25}Mo_{0.25}S_5I$	0.40
	47	$Li_{6.25}Si_{0.5}Sb_{0.25}Mo_{0.25}S_5I$	-0.07
	48	$Li_{6.25}Si_{0.5}Sb_{0.25}W_{0.25}S_5I$	-0.07
Group (4-1)	49	$Li_{6.25}Ge_{0.5}Sb_{0.25}W_{0.25}S_5Br$	0.27
	50	$Li_{6.5}Ge_{0.75}Mo_{0.25}S_5Br$	0.37
	51	$Li_{6.25}Si_{0.5}Sb_{0.25}Mo_{0.25}S_5Br$	-0.08
	52	$Li_{6.5}Ge_{0.75}W_{0.25}S_5Cl$	0.37
	53	$Li_{6.5}Si_{0.75}W_{0.25}S_5Br$	-0.15
	54	$Li_{6.25}Ge_{0.5}Sb_{0.25}Mo_{0.25}S_5Cl$	0.38
	55	$Li_{6.25}Ge_{0.5}Sb_{0.25}Mo_{0.25}S_5Br$	0.38
	56	$Li_{6.25}Si_{0.5}Sb_{0.25}W_{0.25}S_5Br$	-0.10
	57	$Li_{6.25}Ge_{0.5}Sb_{0.25}W_{0.25}S_5Cl$	0.27
	58	$Li_{6.5}Si_{0.75}W_{0.25}S_5Cl$	-0.15
	59	$Li_{6.5}Ge_{0.75}W_{0.25}S_5Br$	0.37
	60	$Li_6Si_{0.75}W_{0.25}S_{4.5}Cl_{1.0}Br_{0.5}$	-0.05
	61	$Li_{6.5}Si_{0.75}Mo_{0.25}S_5Cl$	-0.15
	62	$Li_6Ge_{0.75}W_{0.25}S_{4.5}Cl_{1.0}Br_{0.5}$	0.69
	63	$Li_{6.25}Si_{0.5}Sb_{0.25}W_{0.25}S_5Cl$	-0.10
	64	$Li_{6.5}Ge_{0.75}Mo_{0.25}S_5Cl$	0.37
	65	$Li_{6.25}Si_{0.5}Sb_{0.25}Mo_{0.25}S_5Cl$	-0.08
	66	$Li_{6.5}Si_{0.75}Mo_{0.25}S_5Br$	-0.15
Group (4-2)	67	$Li_{5.75}Ge_{0.5}Sb_{0.25}Mo_{0.25}S_{4.5}Cl_{1.0}Br_{0.5}$	0.55
	68	$Li_{5.75}Ge_{0.5}Sb_{0.25}Mo_{0.25}S_{4.5}Cl_{0.5}Br_{1.0}$	0.55
	69	$Li_6Ge_{0.75}Mo_{0.25}S_{4.5}Cl_{0.5}Br_{1.0}$	0.69
	70	$Li_{5.75}Ge_{0.5}Sb_{0.25}W_{0.25}S_{4.5}Cl_{0.5}Br_{1.0}$	0.55
	71	$Li_{5.75}Si_{0.5}Sb_{0.25}W_{0.25}S_{4.5}Br_{1.0}Cl_{0.5}$	-0.19
	72	$Li_{5.75}Si_{0.5}Sb_{0.25}Mo_{0.25}S_{4.5}Br_{1.0}Cl_{0.5}$	-0.19
	73	$Li_{5.75}Si_{0.5}Sb_{0.25}Mo_{0.25}S_{4.5}Cl_{1.0}Br_{0.5}$	-0.19
	74	$Li_6Si_{0.75}W_{0.25}S_{4.5}Cl_{0.5}Br_{1.0}$	-0.05
	75	$Li_{5.75}Si_{0.5}Sb_{0.25}W_{0.25}S_{4.5}Cl_{1.0}Br_{0.5}$	-0.19
	76	$Li_6Ge_{0.75}W_{0.25}S_{4.5}Cl_{0.5}Br_{1.0}$	0.69
	77	$Li_{5.75}Ge_{0.5}Sb_{0.25}W_{0.25}S_{4.5}Cl_{1.0}Br_{0.5}$	0.55
	78	$Li_6Si_{0.75}Mo_{0.25}S_{4.5}Cl_{1.0}Br_{0.5}$	-0.05
	79	$Li_6Si_{0.75}Mo_{0.25}S_{4.5}Cl_{0.5}Br_{1.0}$	-0.05
Group	80	$Li_{5.75}Ge_{0.75}Mo_{0.25}S_{4.25}Cl_{1.25}Br_{0.5}$	0.72

(4-3)	81	$Li_{5.5}Ge_{0.5}Sb_{0.25}W_{0.25}S_{4.25}Cl_{1.25}Br_{0.5}$	0.54
	82	$Li_{5.5}Si_{0.5}Sb_{0.25}Mo_{0.25}S_{4.25}Cl_{1.25}Br_{0.5}$	-0.20
	83	$Li_{5.5}Si_{0.5}Sb_{0.25}W_{0.25}S_{4.25}Cl_{1.25}Br_{0.5}$	-0.20
	84	$Li_{5.5}Ge_{0.5}Sb_{0.25}Mo_{0.25}S_{4.25}Cl_{1.25}Br_{0.5}$	0.54

References

1. G. L. Hart and R. W. Forcade, *Physical Review B*, 2008, **77**, 224115.
2. G. L. Hart and R. W. Forcade, *Physical Review B*, 2009, **80**, 014120.
3. G. L. Hart, L. J. Nelson and R. W. Forcade, *Computational Materials Science*, 2012, **59**, 101-107.
4. W. S. Morgan, G. L. Hart and R. W. Forcade, *Computational Materials Science*, 2017, **136**, 144-149.
5. Y. Zuo, C. Chen, X. Li, Z. Deng, Y. Chen, J. Behler, G. Csányi, A. V. Shapeev, A. P. Thompson, M. A. Wood and S. P. Ong, *The Journal of Physical Chemistry A*, 2020, **124**, 731-745.
6. S. P. Ong, W. D. Richards, A. Jain, G. Hautier, M. Kocher, S. Cholia, D. Gunter, V. L. Chevrier, K. A. Persson and G. Ceder, *Computational Materials Science*, 2013, **68**, 314-319.
7. A. V. Shapeev, *Multiscale Modeling & Simulation*, 2016, **14**, 1153-1173.
8. I. S. Novikov, K. Gubaev, E. V. Podryabinkin and A. V. Shapeev, *Machine Learning: Science and Technology*, 2021, **2**, 025002.
9. C. Chen, Y. Zuo, W. Ye, Q. Ji and S. P. Ong, 2022.
10. N. Shuichi, *Progress of Theoretical Physics Supplement*, 1991, **103**, 1-46.
11. W. G. Hoover, *Physical Review A*, 1985, **31**, 1695-1697.
12. J. Klimeš, D. R. Bowler and A. Michaelides, *Journal of Physics: Condensed Matter*, 2010, **22**, 022201.
13. C. Wang, K. Aoyagi, P. Wisesa and T. Mueller, *Chemistry of Materials*, 2020, **32**, 3741-3752.
14. J. Qi, S. Banerjee, Y. Zuo, C. Chen, Z. Zhu, M. H. Chandrappa, X. Li and S. P. Ong, *Materials Today Physics*, 2021, **21**, 100463.
15. B. Jun and S. U. Lee, *Journal of Materials Chemistry A*, 2022, **10**, 7888-7895.
16. P. Adeli, J. D. Bazak, K. H. Park, I. Kochetkov, A. Huq, G. R. Goward and L. F. Nazar, *Angewandte Chemie International Edition*, 2019, **58**, 8681-8686.
17. Y. Liu, H. Peng, H. Su, Y. Zhong, X. Wang, X. Xia, C. Gu and J. Tu, *Advanced Materials*, 2022, **34**, 2107346.
18. V. Faka, M. T. Agne, P. Till, T. Bernges, M. Sadowski, A. Gautam, K. Albe and W. G. Zeier, *Energy Advances*, 2023, **2**, 1915-1925.
19. T. Jeon, G. H. Cha and S. C. Jung, *Journal of Materials Chemistry A*, 2024, **12**, 993-1002.
20. Y. Lee, J. Jeong, H.-D. Lim, S.-O. Kim, H.-G. Jung, K. Y. Chung and S. Yu, *ACS Sustainable Chemistry & Engineering*, 2021, **9**, 120-128.
21. J. Qi, S. Banerjee, Y. Zuo, C. Chen, Z. Zhu, M. L. Holekevi Chandrappa, X. Li and S. P. Ong, *Materials Today Physics*, 2021, **21**, 100463.
22. P. Hopkins, A. Fortini, A. J. Archer and M. Schmidt, *The Journal of chemical physics*, 2010, **133**.
23. Z. Zhu, I.-H. Chu, Z. Deng and S. P. Ong, *Chemistry of Materials*, 2015, **27**, 8318-8325.
24. C. H. Chen and K. Amine, *Solid State Ionics*, 2001, **144**, 51-57.
25. Y. Zhu, X. He and Y. Mo, *Journal of Materials Chemistry A*, 2016, **4**, 3253-3266.